Nanoscale

ROYAL SOCIETY OF CHEMISTRY

PAPER

View Article Online
View Journal | View Issue

Cite this: *Nanoscale*, 2023, **15**, 17899

Nanobubble-mediated cancer cell sonoporation using low-frequency ultrasound†

Mike Bismuth, [a] Michal Eck[a] and Tali Ilovitsh *[a,b]

Ultrasound insonation of microbubbles can form transient pores in cell membranes that enable the delivery of non-permeable extracellular molecules to the cells. Reducing the size of microbubble contrast agents to the nanometer range could facilitate cancer sonoporation. This size reduction can enhance the extravasation of nanobubbles into tumors after an intravenous injection, thus providing a noninvasive sonoporation platform. However, drug delivery efficacy depends on the oscillations of the bubbles, the ultrasound parameters and the size of the target compared to the membrane pores. The formation of large pores is advantageous for the delivery of large molecules, however the small size of the nanobubbles limit the bioeffects when operating near the nanobubble resonance frequency at the MHz range. Here, we show that by coupling nanobubbles with 250 kHz low frequency ultrasound, high amplitude oscillations can be achieved, which facilitate low energy sonoporation of cancer cells. This is beneficial both for increasing the uptake of a specific molecule and to improve large molecule delivery. The method was optimized for the delivery of four fluorescent molecules ranging in size from 1.2 to 70 kDa to breast cancer cells, while comparing the results to targeted microbubbles. Depending on the fluorescent molecule size, the optimal ultrasound peak negative pressure was found to range between 300 and 500 kPa. Increasing the pressure to 800 kPa reduced the fraction of fluorescent cells for all molecules sizes. The optimal uptake for the smaller molecule size of 4 kDa resulted in a fraction of 19.9 ± 1.8% of fluorescent cells, whereas delivery of 20 kDa and 70 kDa molecules yielded 14 ± 0.8% and 4.1 ± 1.1%, respectively. These values were similar to targeted microbubble-mediated sonoporation, suggesting that nanobubbles can serve as noninvasive sonoporation agents with a similar potency, and at a reduced bubble size. The nanobubbles effectively reduced cell viability and may thus potentially reduce the tumor burden, which is crucial for the success of cancer treatment. This method provides a non-invasive and low-energy tumor sonoporation theranostic platform, which can be combined with other therapies to maximize the therapeutic benefits of cancer treatment or be harnessed in gene therapy applications.

Received 3rd July 2023,
Accepted 20th October 2023

DOI: 10.1039/d3nr03226d

rsc.li/nanoscale

1. Introduction

The development of intravenously (IV) injected microbubbles (MBs), with an average diameter of 1.5–4 μm, has greatly enhanced the applications of ultrasound (US) beyond soft tissue imaging to functional intravascular imaging,[1] and also to therapeutic applications, as demonstrated with compelling research reporting notable bioeffects.[2–4] MBs formed of a gas core and a stabilizing shell are efficient US theranostic probes that serve as both contrast and therapeutic agents. Upon US excitation, MBs cavitate and pulsate volumetrically, applying mechanical forces and transiently forming pores in adjacent cell membranes that can promote local drug and gene delivery.[5,6] After insonation, the cell membrane pores close and revert to their original state, so that the therapeutic material becomes confined within the cell.[7,8] This method, termed sonoporation, is a promising targeted, nonviral and non-toxic gene and drug delivery method[9–11] and offers the benefits associated with US (safety, user-friendliness, relative low cost, and widespread clinical accessibility).[12] Due to the noninvasive nature of US, it can be applied directly to deep-seated organs with site-specificity, enabling sonoporation of deep tissues with negligible off-target effects.[13,14]

Until recently, the large size of MBs restrained them to intravascular applications, since they were too big to extravasate from the blood vessels into the surrounding tissue.[2,15,16] The development of nanobubbles (NBs) has expanded gas-bubble effects beyond the vascular compartment because of their small size (less than 500 nm) that enables effective tumor uptake *via* the leaky tumor vasculature.[17–19] In sonoporation

[a]*Department of Biomedical Engineering, Tel Aviv University, Tel Aviv 6997801, Israel. E-mail: ilovitsh@tauex.tau.ac.il*
[b]*The Sagol School of Neuroscience, Tel Aviv University, Tel Aviv 6997801, Israel*
† Electronic supplementary information (ESI) available. See DOI: https://doi.org/10.1039/d3nr03226d

studies, NBs have been employed for the delivery of drugs and genes at high frequencies.[20,21] However, the effective delivery of large molecules requires sufficiently high-amplitude NBs oscillations to apply enough mechanical force to generate large pores in adjacent cell membranes.[22] In the past, NBs were typically excited at high US frequencies of tens of MHz.[23,24] These frequencies were shown to improve resolution and facilitate NB imaging.[25] In addition, since the bubbles' resonance frequency is inversely proportional to their diameter, NBs' resonance frequency is high (40 MHz for a 200 nm NB).[26,27] Nevertheless, at these frequencies, strong NB oscillations do not occur.[20] Sonoporation that requires strong cavitation thus remained a significant challenge. We recently showed that exciting MBs with low frequency US of 250 kHz, well below their resonance frequency, triggers their high amplitude oscillations as a result of the Blake threshold effect.[28–32] By exploiting this effect, we developed MB-mediated sonoporation for large molecules delivery to cancer cells.[33] For tumor therapy application *in vivo*, the MB were intratumorally injected, making it an invasive approach.[32] In addition, we showed that since MBs are buoyant and close proximity to the cells is required, targeted MBs (TMBs) were used.[32,33] Here we report the development of a noninvasive NB-mediated cancer cell sonoporation platform. Recently we showed that the Blake threshold is also applicable to nanoscale bubbles, and causes violent NB oscillations at center frequencies below 250 kHz. This discovery was used for the development of NB-mediated low energy mechanical ablation of tumors.[19] Here, we present the use of low-frequency mediated NB insonation for the promotion of cancer cell large pore formation as a sonoporation platform. Cancer cell sonoporation is particularly challenging and requires stronger oscillations than other cell types.[34,35] In cancer treatment, tumor burden reduction is key for effective therapy.[36,37] Thus, in addition to improved drug delivery, our goal was also to reduce cell viability. Sonoporation depends on factors such as the size of the generated membrane pores, the US parameters and the delivered particle size.[5,38] NB-mediated sonoporation was optimized through the delivery of 4 fluorescent molecules ranging from 1.2 to 70 kDa in size and results were compared to the gold standard TMB-mediated sonoporation.

2. Results

2.1. Delivery of 7-AAD

We first tested the 7-Aminoactinomycin D (7-AAD) molecule, which has a molecular weight of 1.2 kDa. Based on our previous work that optimized the 7-AAD concentration and incubation time, the concentration used here was 5 μg ml^{-1} and a time point of 0 was used for fluorescence microscopy analysis (*e.g.* immediately post-US treatment).[33] 7-AAD is a fluorescent dye that undergoes a spectral shift upon association with DNA. Therefore, after sonoporation, the fluorescent signal only emanates from the stained cells and does not exist in the background suspension. Consequently, fluorescence microscopy can be used immediately after the treatment to visualize and quantify the percentage of fluorescent cells. The images presented in Fig. 1A are an overlay of both Hoechst and 7-AAD stained cells. The Hoechst-stained cells marked in blue represent the total cells in the sample. The 7-AAD positive cells appear pink. The objective of this experiment was to provide preliminary evidence of the ability of NBs, when combined with a low frequency US of 250 kHz, to produce a large enough bioeffect and permit significant sonoporation. There was a similar percentage of fluorescent cells in the sham (15.3 ± 7.8%), and NB only (18.1 ± 4.3%). The fraction of 7-AAD stained cells increased significantly after NBs-mediated treatment in comparison to the control groups and reached values of 61.4 ± 12.8% and 61.6 ± 8.3% for 800 kPa and 1350 kPa treatments respectively ($p < 0.01$, $p < 0.001$) (Fig. 1B).

2.2. Nanobubble concentration calibrations

In vitro experiments were performed to assess the impact of NB low frequency insonation (250 kHz) on cancer cell uptake

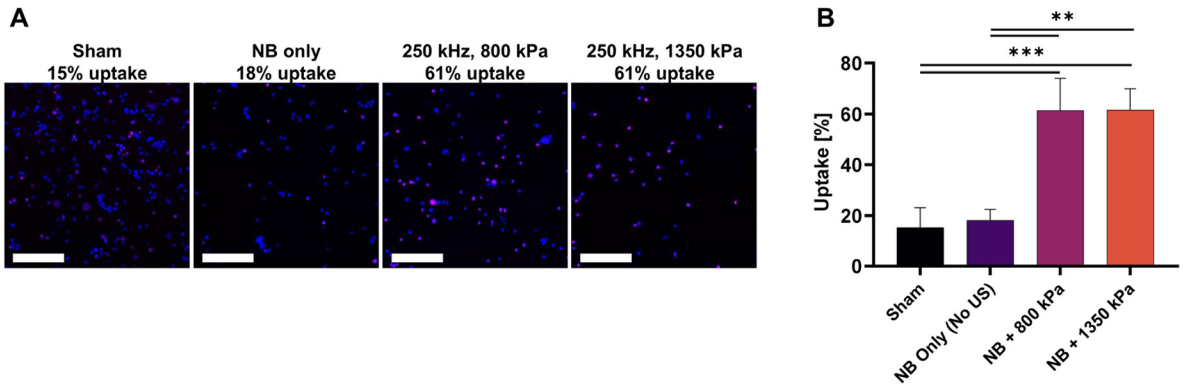

Fig. 1 7-AAD delivery to breast cancer cell experiments. (A) Fluorescence microscopy images for sham, nanobubbles only and different ultrasound treatment groups. Images are an overlay of both Hoechst and 7-AAD stained cells. Hoechst-stained cells (the total cells in the sample) are blue and the 7-AAD positive cells appear pink. Images were acquired at 10× magnification. The scale bar is common to all subfigures in (A) and was 200 μm. (B) 7-AAD stained cells are expressed as the percentage of total cells for the different treatment and control groups. A one-way ANOVA with Tukey's multiple comparison test was conducted. The adjusted p values were $^{**}p < 0.01$, $^{***}p < 0.001$. All data are plotted as the mean ± SD.

as a function of NB concentration. Eppendorf tubes containing a mixture of NBs, FITC 4 kDa and breast cancer cells were insonated using low frequency US. In our previous study, we assessed the NB-mediated mechanical ablation effectiveness of various treatment durations *in vitro*. However, there was no notable discrepancy for the different durations tested (30, 60, and 90 seconds). As a result, to limit US exposure, we opted for a treatment duration of 30 seconds.[19] Unlike 7-AAD, FITC-dextran fluoresces on its own, and there was a high background signal in the suspension immediately after treatment. In order to remove this fluorescence background, after the US treatment, the cell suspension was cultured for a further 24 h in plates. During this time, the cells adhered to the plate, and the media were washed and replaced to remove all of the fluorescent background signal. Hence, 4, 20 and 70 kDa FITC-dextrans fluorescence and viability tests were performed 24 h post treatment. Cancer cell uptake was assessed at a constant pressure of 300 kPa for all concentrations tested. The initial concentration was $x = 1.29 \times 10^7$ NBs per μL, and 5 other concentrations of 2, 4, 8, 12 and 16 times the initial concentration were tested. No significant FITC 4 kDa uptake difference was found across the different control groups. The sham group exhibited 2.9 ± 2.5% uptake, the free MB, with a concentration of 50 MBs per cell, resulted in 5.1 ± 1.3% uptake and the NBs only (at the optimal NB concentration of 12×) resulted in 1.5 ± 0.3% uptake. The proportion of fluorescent cells increased as a function of the concentration of NBs until a concentration of 12× was reached (at which point the highest proportion of fluorescent cells was 17.9 ± 5.5%). However, above this concentration, the fraction of fluorescent cells began to decline, reaching 11.7 ± 2% at a concentration of 16× (non-significant, $p > 0.05$) (Fig. 2B). These results suggest that 12× was the optimal NB concentration for the delivery of FITC 4 kDa molecules.

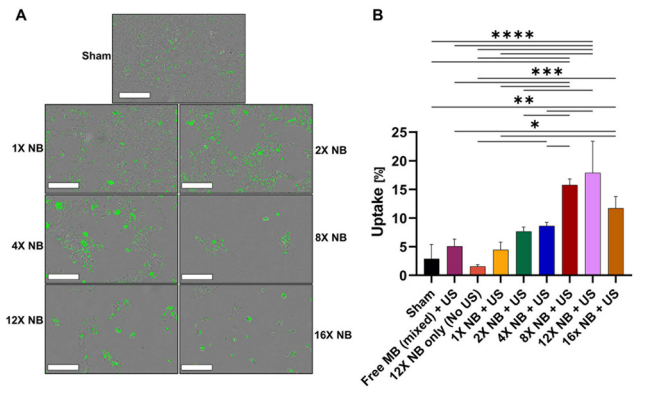

Fig. 2 Nanobubble concentration optimization for 4 kDa FITC delivery. (A) Overlay images of cells and the FITC 4 kDa fluorescent signals for different nanobubble concentration groups at a constant pressure of 300 kPa. Cells were imaged one day after sonoporation treatment. Images were acquired by the Incucyte system at 20× magnification. Scale bars are 200 μm in all subfigures. (B) Impact of nanobubble concentrations on FITC 4 kDa cellular uptake expressed as the percentage of the total cells. A one-way ANOVA with Tukey's multiple comparison test was conducted. The adjusted p values were $*p < 0.05$, $**p < 0.01$, $***p < 0.001$, $****p < 0.0001$. All data are plotted as the mean ± SD.

2.3. Delivery of FITC 4 kDa

Here, we evaluated how US level pressure applied on NBs during sonoporation treatment affected the uptake of 4 kDa FITC-dextran by breast cancer cells. We maintained a consistent FITC-dextran concentration of 1 mg ml^{-1} for all sizes tested in this experiment, which was selected based on previous investigations.[39–42] The percentage of fluorescent cells increased as a function of the applied peak negative pressures (PNP) during the treatment with NBs, reaching a maximum uptake of 19.9 ± 1.8% at a PNP of 500 kPa. Beyond this pressure, the fraction of fluorescent cells decreased, with a 13.8 ± 1.6% uptake observed at a PNP of 800 kPa (non-significant, $p > 0.05$) (Fig. 3B). The 4 kDa FITC uptake percentage was 4.1 ± 0.2% and 8.9 ± 0.6% for the sham and 200 kPa groups, respectively. These findings indicate that a PNP of 500 kPa was the optimal pressure for delivering these molecules. However, no significant difference was observed in uptake percentage between 300 kPa and 500 kPa. When compared with sonoporation results achieved through TMB-mediated treatment, the results obtained from NBs treatment for the same pressures showed no significant difference (not significant, $p > 0.05$), except for the 800 kPa TMB and NB groups where uptake ratios obtained were 24.1 ± 5.5% and 13.8 ± 1.6% respectively ($*p < 0.05$). The uptake in the US only group (0.22 ± 0.13%) did not show a significant difference when compared to the sham group (non-significant, $p > 0.05$).

2.4. Delivery of FITC 20 kDa

Next, the size of the delivered molecule was increased to FITC-dextran 20 kDa. The pressures evaluated were the same as used for the FITC-dextran 4 kDa sonoporation (200 kPa, 300 kPa, 500 kPa and 800 kPa). At a PNP of 300 kPa, the uptake of FITC-dextran 20 kDa reached its maximum of 14 ± 0.8%. However, beyond this pressure, the fraction of fluorescent cells decreased, with a 10.3 ± 3.4% and 5.4 ± 2.7% uptake observed at 500 kPa and 800 kPa respectively. In the sham group, the percentage of fluorescent cells was 2.9 ± 1.4%, which increased to 8.3 ± 2.3% at a PNP of 200 kPa (Fig. 4B). These results suggest that 300 kPa is the optimal pressure for delivering these molecules. Resulting uptakes were lower for FITC 20 kDa in comparison to FITC 4 kDa for all pressure tested. In terms of sonoporation results achieved through TMB-mediated treatment, there was no significant difference in uptake between NBs treatment and TMBs treatment for the same pressures (not significant, $p > 0.05$), except for the 800 kPa group where the uptake ratios were 13.2 ± 1.6% for MBs and 5.4 ± 2.7% for NBs ($*p < 0.05$).

2.5. Delivery of FITC 70 kDa

Finally, the size of the delivered molecule was increased to FITC-dextran 70 kDa. The pressures tested were unchanged. The 4T1 cells reached optimal FITC 70 kDa uptake at a PNP of 300 kPa and 500 kPa where the maximal fractions of fluo-

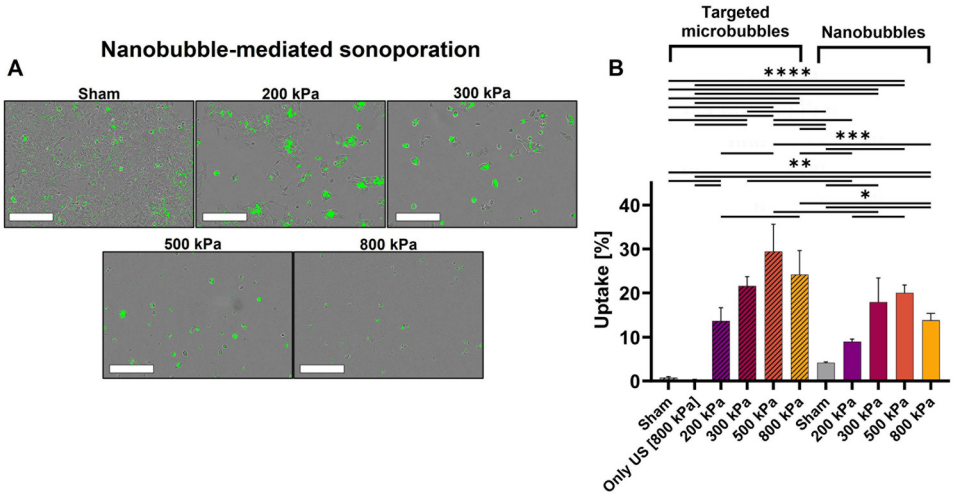

Fig. 3 FITC 4 kDa sonoporation results. (A) Overlay images of cells and FITC 4 kDa fluorescence for different peak negative pressure groups with a constant nanobubble concentration of 12×. Cells were imaged one day after sonoporation treatment. Images were acquired by the Incucyte system at 20× magnification. Scale bars are 200 μm in all subfigures. (B) Impact of peak negative pressure on FITC 4 kDa cellular uptake expressed as the percentage of the total cells for targeted microbubbles[33] and nanobubbles. A one-way ANOVA with Tukey's multiple comparison test. Adjusted p values were *$p < 0.05$, **$p < 0.01$, ***$p < 0.001$, ****$p < 0.0001$. All data are plotted as the mean ± SD.

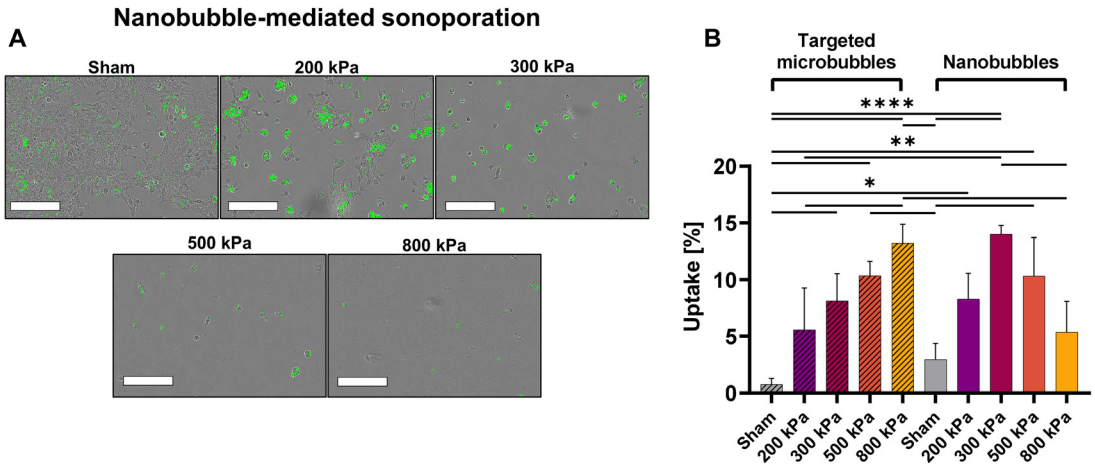

Fig. 4 FITC 20 kDa sonoporation results. (A) Overlay images of cells and FITC 20 kDa fluorescence for different peak negative pressure groups with a constant nanobubble concentration of 12×. Cells were imaged one day after sonoporation treatment. Images were acquired by the Incucyte system at 20× magnification. Scale bars are 200 μm in all subfigures. (B) Impact of peak negative pressure on FITC 20 kDa cellular uptake expressed as the percentage of the total cells. Targeted microbubble results[33] were incorporated into the graph displaying the results from the nanobubble treatment for comparison. A one-way ANOVA with Tukey's multiple comparison test was conducted. The adjusted p values were *$p < 0.05$, **$p < 0.01$, ****$p < 0.0001$. All data are plotted as the mean ± SD.

rescent cells were 4.1 ± 1.1%. Beyond these PNPs, the fraction of fluorescent cells dropped to 1.8 ± 1.1% for a PNP of 800 kPa (non-significant, $p > 0.05$). The 70 kDa FITC uptake percentage was 1.3 ± 0.6% and 2.6 ± 1% for the sham and 200 kPa groups, respectively (Fig. 5B). The resulting uptakes were lower for FITC 70 kDa in comparison to the FITC 20 kDa and FITC 4 kDa for all pressures tested. When compared to the sonoporation results for TMB-mediated treatment, the results for the NB treatment for the same pressures showed no significant difference for all groups tested (non-significant, $p > 0.05$).

2.6. Cell viability post treatment

Cell viability was evaluated for the treatment groups 24 h post-sonoporation at the same time point used for FITC molecule uptake evaluation. To enable comparison, the TMB results obtained in our previous work[33] were included in the graph displaying the results for the NBs treatment. Viability was also assessed for NB only and TMB only (no US application). Viability dropped to 23.7 ± 0.7% for the treatment only with TMB. However, no significant difference was found between

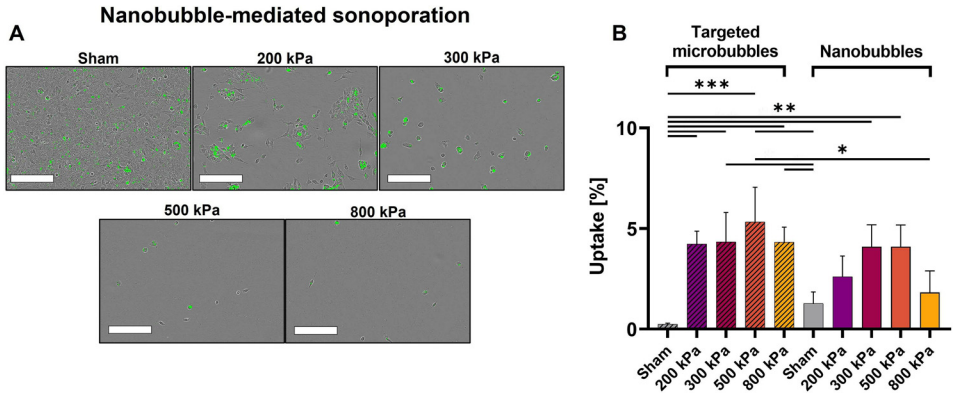

Fig. 5 FITC 70 kDa sonoporation results. (A) Overlay images of cells and FITC 70 kDa fluorescence for different peak negative pressure groups with a constant nanobubble concentration of 12×. Cells were imaged one day after sonoporation treatment. Images were acquired by the Incucyte system at 20× magnification. The scale bars are 200 μm in all subfigures. (B) Impact of peak negative pressure on FITC 70 kDa cellular uptake expressed as the percentage of the total cells. Targeted microbubble results[33] were incorporated into the graph displaying the results for the nanobubble treatment for comparison. A one-way ANOVA with Tukey's multiple comparison test was conducted. The adjusted p values were *$p < 0.05$, **$p < 0.01$, ***$p < 0.001$. All data are plotted as the mean ± SD.

the only-NB group, the sham group and the only US group (100 ± 4.8%, 102.3 ± 5.7%, and 110.2 ± 5.4%, respectively, non-significant, $p > 0.05$). The PNP used in the only US group was 800 kPa. This PNP is the highest pressure tested across all the FITC groups in our work. To confirm that the reduction in viability observed in the group treated exclusively with TMBs is not a result of cell buoyancy following TMB binding which might limit their attachment to the plate, we conducted an experiment to assess the stability of the TMBs when attached to 4T1 cells under the same experimental conditions as the uptake experiments, at three time points: 0, 1, and 2 hours. The number of TMBs on the cells dropped significantly after one hour, and no TMBs were found after two hours (Fig. S1†). The NB-mediated results showed no significant difference for all groups tested (Fig. 6, non-significant, $p > 0.05$) when compared to the viability results for the TMB-mediated treatment, except for the 200 kPa treatment. In this case, the viability for the NB group was significantly higher than the TMB group (42.2 ± 1.6% *vs.* 11.3 ± 1.6%, ****$p < 0.0001$). Our viability evaluation was based on the cells confluency calculated by the Incucyte Live-Cell Analysis System (Essen Bioscience). This approach eliminated the need to harvest cells from the plate and reduced the potential for human errors resulting from manual handling. To further affirm the validity of our cell viability evaluation method, we compared our results with cell viability rates resulting from a cell counting instrument (CellDrop, DeNovix Inc., Wilmington, USA). In these experiments, cells were collected from the wells and counted using the cell counter. The results obtained from both of these survival evaluation methods were similar, with no statistically significant differences between them (Fig. S2,† not significant, $p > 0.05$).

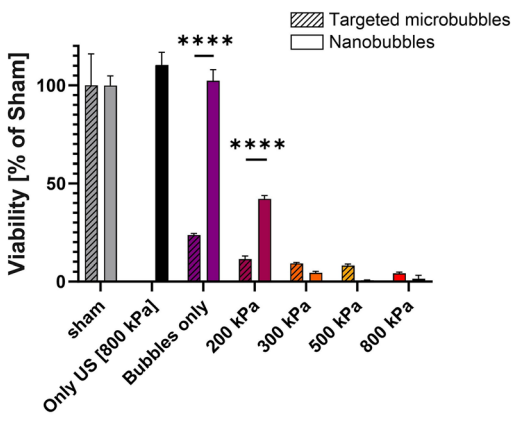

Fig. 6 Cell viability post-sonoporation treatment. Viability of cells expressed as the percentage of the sham group for the different treatment and control groups 1 day after sonoporation with FITC 4 kDa. Targeted microbubble results[33] were incorporated into the graph for comparison. A one-way ANOVA with Tukey's multiple comparison test was conducted. Adjusted p values were ns $p > 0.05$, **** $p < 0.0001$. All data are plotted as the mean ± SD.

3. Discussion

The field of sonoporation is expanding and has demonstrated efficacy in delivering drugs and genes to diverse cell types and tissues.[6,8,43] This method has several advantages over other delivery techniques, in that it is cost effective, deep penetrating and widely available.[13,44,45] Compared to biological techniques such as viral vectors, sonoporation enhances the spatiotemporal precision of gene delivery and can considerably reduce undesirable side effects and non-specific toxicity.[46]

For cancer treatment applications, a significant number of cancer cells must undergo sonoporation, and a high delivery efficacy is needed to maximize the drug concentration within the cells. Our approach to achieving a high sonoporation rate involves utilizing low frequency insonation, unlike the majority of optimization studies in this field that have utilized frequencies exceeding 1 MHz, where strong MB oscillations require PNP that exceed the Food and Drug Administration's (FDA)

safety threshold.[31,47–49] Low frequency insonation was shown to increase gas bubble oscillations, which was used here to enhance sonoporation.[31] In addition, low-frequency US has the advantage of lower attenuation compared to high frequencies, allowing for greater penetration of deep-seated organs. With a fixed aperture, lowering the US frequency enlarges the focal spot size, allowing the simultaneous treatment of a larger tumor volume. If necessary, adjusting the transducer aperture can be employed to shrink the focal zone size, enabling more precise targeting of the tumor.[50–52] In brain therapy applications, a lower frequency is advantageous in achieving focused targeting through the human skull with minimal distortion and attenuation, as highlighted by the clinical trials currently in progress for a variety of brain diseases.[52–55] Based on the Blake threshold effect, the use of low frequency US was found to generate large NBs oscillation permitting NBs-mediated therapeutic applications despite their reduced size.[19,29] Here, we described an enhanced sonoporation platform using NBs with a mean diameter of 170 nm that can be systemically injected. This overcomes current sonoporation limitations that stem from the large MB diameter used in most sonoporation studies. In addition, the low energies applied do not induce heat, so that the effect remains purely mechanical.

In the case of cancer therapy, high delivery efficacy and reducing cell viability are equally important. This is because minimizing the tumor burden is essential for the success of cancer treatment.[36,37,56] For this reason, in this study we aim to achieve multiple outcomes, including enhanced drug delivery, reduced tumor burden, and decreased cell viability in order to improve cancer therapy, which is our overreaching goal. Although this article dealt with the sonoporation of cancer cells, future applications could include the sonoporation of other cell types, such as immune cells, muscle cells and endothelial cells. This method could also be applied for gene therapy, where the goal is to introduce new genetic material into cells.

Here, we investigated the delivery of 4 different fluorescent molecules ranging in size from 1.2 kDa to 70 kDa, which corresponds to substances such as chemotherapeutic drugs (1–70 kDa), siRNA (~14 kDa), and proteins (3–40 kDa).[22,57–62] Due to the physical dimensions of the transducer's focal spot, the experiments were carried out in Eppendorf tubes. For the 250 kHz center frequency, the lateral and axial axes had a full width at half maximum of 7 × 50 mm. The elongated shapes of the Eppendorf and focal point were utilized to carry out the treatment in these tubes, because they allow for the simultaneous treatment of the entire volume without having to mechanically move the transducer, as would be the case if using adherent cells in plates. The initial cell culturing was carried out in plates. After undergoing US treatment, the cells were then transferred back to the 24-well plates. The control groups underwent the same procedures as the treated groups. The initial molecule examined in this study was the 7-AAD (1.2 kDa). 7-AAD is a membrane-impermeable dye that undergoes a spectral shift upon binding to DNA. During the sonoporation process, pores can form in the cell membrane, allowing 7-AAD to enter the cells. The use of suspended cells likely increases the chances of 7-AAD entering untreated cells and given enough time, this dye can spontaneously permeate cells as we can see in the relative high uptake in sham and NB only groups (Fig. 1). This parameter was previously optimized (ref. 33). Our goal here was to provide preliminary evidence for the ability of free NB-mediated sonoporation using low frequency US. The results demonstrated a significant increase in the uptake ratio after treatment (Fig. 1A and B). It's worth noting that since these cells were imaged immediately after treatment, some may not have been viable. Next, the delivery of larger FITC molecules with molecular weights of 4 kDa, 20 kDa, and 70 kDa was optimized by studying the impact of PNP on sonoporation efficacy and cell viability.

In contrast to 7-AAD, which provides a fluorescent signal exclusively from stained cells and doesn't introduce background fluorescence in the suspension, FITC-dextran has its own fluorescence and contributes to a high background signal immediately after treatment. To mitigate this, after the US treatment, the cell suspension was cultured for an additional 24 hours in plates. During this period, cells adhered to the plate, allowing us to wash and replace the media to eliminate any remaining fluorescent background signal. Non-viable cells remained in the suspension and did not adhere, making the FITC-delivery experiments a more precise metric to assess cell viability and molecular uptake.

The percentage of fluorescent cells was utilized as a yardstick to assess delivery efficiency and to compare the different sizes of FITC. For uptake evaluation, the calculation procedure involved normalizing the green confluence (representing FITC-dextran uptake) by the phase confluence (indicating the total cell area). The highest rate of fluorescent cells resulting from NB sonoporation was observed for the smallest molecules, with approximately 19.9 ± 1.8% of the live cells for the FITC 4 kDa molecule (Fig. 3B). For FITC molecules weighing 20 and 70 kDa, the percentage of fluorescent cells was 14 ± 0.8% and 4.1 ± 1.1% of the live cells, respectively (Fig. 4B and 5B). This pattern is in line with the results obtained for TMB-mediated sonoporation, where uptake was diminished for larger molecules.[33] In these experiments, we implemented a sham control group that was subjected to the exact same conditions as the treatment groups, including incubation with FITC. If any cells took up FITC during the 24-hour incubation period, this would result in an increase across all groups. Upon comparison, we observed that the NB-mediated sonoporation group exhibited significantly higher FITC uptake compared to the sham group. Moreover, the phase contrast and fluorescence images of the cells obtained using the IncuCyte Live-Cell Analysis System consistently depicted live cells firmly adhered to the plate surface. As a result, it is reasonable to anticipate that all the experimental groups exhibited a comparable degree of autofluorescence.

To aid in preventing damage to healthy tissue during diagnostic US, the upper limit of the mechanical index (MI) was defined as 1.9 by the FDA. The MI was originally defined for

frequencies higher than 800 kHz. Nevertheless, we opted to use it in the absence of an alternative safety metric for low-frequency therapeutic US. Here, an upper PNP limit of 800 kPa resulting in an MI of 1.6 was chosen. This was done to ensure that the PNP remained below the FDA's MI limit. In a recent publication we showed that low frequency insonation of tumors without NBs at these settings did not cause mechanical damage to the tumor and that our treatment combining low frequency US and NBs did not impact other internal organs.[19]

The optimal uptake was observed between 300 kPa and 500 kPa, and no significant difference was found between these pressures for all the tested FITC sizes. Increasing the PNP to 800 kPa led to decreased uptake for all FITC molecules tested (Fig. 3B, 4B and 5B). The NB concentrations were calibrated for FITC 4 kDa sonoporation at a fixed pressure of 300 kPa for all tested concentrations. The initial concentration of NBs was 1.29×10^7 NBs per μL, and five additional concentrations (2, 4, 8, 12, and 16 times the initial concentration) were tested. The optimal concentration of NBs was found to be 12 times the initial concentration, since higher concentration decreased the uptake. It should be noted that that our optimal concentration of 12× was tailored to our specific setup and may exhibit variations when applied in different experimental configurations. The results showed that the combination of US and NBs increased cellular uptake significantly compared to all the other control groups including sham ($p < 0.0001$), free MBs (mixed) + US ($p < 0.0001$) and 12× NB only ($p < 0.0001$). In addition, the uptake after free MB insonation was slightly higher than the sham group, but the results were not significant ($p > 0.05$) (Fig. 2B). It should be noted that there is a significant difference between MBs and NBs in the context of *in vitro* assays, because proximity to the cells plays a crucial role.[33,63] MBs tend to float, which accounts for the lack of increased uptake after free MBs insonation. In a previous study, it was shown that free MBs + US did not affect cell viability.[32] To achieve close proximity to the cell membrane, cell-targeted MBs were used. In contrast, NBs are neutrally buoyant and move in Brownian motion within the suspension,[64] so that the NBs used in this study were free and untargeted. One of the key objectives of this research was to investigate how the molecular size of fluorescence molecules influences their cellular uptake when subjected to sonoporation. By maintaining the NB concentration identical across the multiple FITC molecules delivery experiments, we could isolate the specific influence of molecular size on cellular uptake. To maximize the uptake of each individual molecule, it may be necessary to adjust the NB concentration. However, increasing the concentration might lead to a further reduction in cell viability. Therefore, finding a balance between molecule uptake and cell viability will be essential.

NB-mediated sonoporation was able to achieve a similar sonoporation efficacy as TMB for the same pressures and all groups tested ($p > 0.05$). The only exceptions were the 800 kPa pressures for FITC 4 and 20 kDa, where the TMBs groups showed significantly higher uptake ratios ($*p < 0.05$). However, the maximal uptake was observed at lower PNPs (300–500 kPa) (Fig. 3B, 4B and 5B). These results suggest that although NBs are smaller in diameter by an order of magnitude compared to TMB, they evidence similar sonoporation abilities, whereas NBs were free and did not require any targeting procedures unlike the TMBs. The TMB concentration in each 0.5 mL Eppendorf tube before the US treatment was 2.6×10^4 TMBs per μl. This translates to an estimated ratio of approximately 5960 NBs/TMBs. However, several factors constrain the validity of this comparison. Firstly, this ratio was calculated based on the concentrations of NBs and TMBs obtained from our AccuSizer FX-Nano particle sizing system, which is unable to differentiate between bubbles and liposomes. Therefore, the actual concentration of NBs is likely lower, potentially altering the NBs/TMBs ratio. Additionally, it's worth noting that NBs are non-targeted in contrast to TMBs. As a result of their close cell proximity and their larger gas volume, it is likely that the TMB exhibit a more potent effect. A direct comparison could be made using targeted NBs, which might reduce the NB concentration.

In terms of cell viability, viability decreased to 22.87 ± 1.01% with treatment using TMBs alone, while the only NBs group showed no significant difference compared to the sham group (102 ± 1%), which suggests that NBs are less toxic than TMBs (Fig. 6). Since the viability assessment was conducted after 24 hours and due to the low stability of the TMBs attached to the cells (Fig. S1†), the TMB only group had enough time to attach to the plate. The viability results of the NBs treatment at the same pressures showed no significant difference for all groups tested (non-significant, $p > 0.05$) compared to the viability results with the TMB-mediated treatment, except for the 200 kPa treatment. At this pressure, the viability for the NB group was significantly higher than the TMB group (42.2 ± 1.6% *vs.* 11.3 ± 1.6%, $****p < 0.0001$) (Fig. 6). This high viability rate with a significant uptake at 200 kPa may be useful in gene therapy applications that require high survival rates and uptake to modify target cells such as immune cells, muscle cells and endothelial cells. Several limitations of this study require mention. The first is that it did not explore the impact of molecular targeting on NBs, which could potentially further enhance the method and will be explored in future studies. It also did not explore the delivery of therapeutic molecules but instead used fluorescent markers of different sizes as a proxy for sonoporation efficacy. Sonoporation of drugs or genetic material should be studied in future work. Finally, the method was only verified *in vitro*. *In vivo*, several additional factors may impact the effectiveness of sonoporation, including the viscoelasticity of the surrounding media,[6] the shape and connections of the cells,[65] and various other variables. Moreover, the NB concentration within the tumor will likely to be different, and this will be optimized as part of a follow up study. However, we can say that in a previous work that focused on mechanical fractionation of tumors using NBs, we were able to achieve significant bioeffects with a systemic injection of NBs (ref. 19). Therefore, we can anticipate that a sufficient amount of NBs can reach the tumor for sonopora-

tion. Moreover, previous studies involving US insonation below 250 kHz have demonstrated a strong correlation between *in vitro* and *in vivo* outcomes.[3,19,32] The optimization results presented here will be applied to future *in vivo* research which will evaluate the delivery efficiency of NBs-mediated low-energy sonoporation when combined with low-frequency US specifically in a mouse tumor model.

4. Conclusions

In this study, we developed a low-frequency NB-mediated sonoporation method and optimized the relationship between insonation parameters and the size of the delivered molecule. Using the same acoustical configuration for all molecules tested enables direct comparisons of uptakes for these molecules. Our work can thus serve as an effective platform for non-invasively delivering large molecules with high spatiotemporal precision. The results indicated that the optimal PNP for delivering molecules with a center frequency of 250 kHz was between 300 kPa and 500 kPa. The highest percentage of fluorescent cells was observed for the smallest molecule, which decreased as the molecule size increased. Overall, the use of a low frequency and a low MI enables the efficient delivery of molecules of different sizes, while reducing cancer cell viability. This approach could thus be used in the future as a combined method to maximize the therapeutic benefits of cancer treatment.

5. Experimental methods

5.1. Microbubble and nanobubble synthesis

NB synthesis was performed as described in.[19,66] 1,2-Dibehenoyl-*sn-glycero*-3-phosphocholine (C22), 1,2-dipalmitoyl-*sn-glycero*-3-phosphate (DPPA), 1,2-dipalmitoyl-*sn-glycero*-3-phosphoethanolamine (DPPE), and 1,2-distearoyl-*sn-glycero*-3-phosphoethanolamine-*N*-[methoxy(polyethylene glycol)-2000] (ammonium salt) (DSPE-mPEG 2000) (Sigma-Aldrich) were dissolved in propylene glycol through a process involving heating to 80 °C and sonicating. Before being added to the lipid solution, glycerol was combined with a preheated phosphate buffered saline (PBS) solution at 80 °C. The final lipid concentration obtained was 10 mg mL^{-1} with a lipids molar ratio of 18.8 : 4.2 : 8.1 : 1. The solution was finally sonicated for 10 minutes at room temperature. A 2 mL headspace vial was used to transfer 1 mL of the resulting solution, which was then saturated with octafluoropropane (C_3F_8) gas. After capping and sealing the vials with a rubber septum and an aluminum seal, they were stored at 4 °C until use. Before experiments, the vial was shaken for 45 seconds for activation using a Vialmix shaker (Bristol-Myers Squibb Medical Imaging Inc., N. Billerica, MA). The inverted vial was then centrifuged (5810R centrifuge, Eppendorf AG, Hamburg, Germany) at 50 g for 5 minutes. Using a 21 G needle, 200 μL of the NB solution was drawn from the inverted vial, approximately 5 mm from the bottom. The MBs and TMBs used in the control groups were synthesized according to.[3,32,33] The sizes and concentrations of the purified MBs, TMBs and NBs were measured using the AccuSizer FX-Nano particle sizing system (Particle Sizing Systems, Entegris, MA, USA). The mean diameters of the NBs and MBs were found to be 170 ± 60 nm and 1.67 ± 0.97 μm, respectively. The bubbles were used within three hours of preparation and the size distributions and concentrations showed variations of less than 10% between measurements.

5.2. Cell preparation

The 4T1 cells, a triple negative murine breast carcinoma cell line characterized by metastatic behavior, were acquired from ATCC (CRL-2539). The cells were grown in T75 tissue culture flasks, which contained RPMI 1640 L-Glutamine (+) supplemented with 10% fetal bovine serum and 1% penicillin–streptomycin. The culture was maintained at 37 °C in a humidified 5% CO_2 incubator. On the day of each experiment, the cell confluency reached approximately 85%. TrypLE Express dissociation reagent (Gibco Corp, 12604-013, Grand Island, NY, USA) was used for cells collection. The cells were then suspended in degassed PBS containing calcium and magnesium (PBS+/+) at a concentration of 6.67×10^6 cells per mL. Cells were counted using the CellDrop device (DeNovix Inc., Wilmington, USA).

5.3. Low frequency ultrasound setup

The US setup was described in.[3,19,33] Briefly, a 0.5 mL Eppendorf tube containing 4T1 cells, NBs and fluorescent molecules in PBS+/+ was placed at the focal point of a single-element transducer with spherical focusing (H115, Sonic Concepts, Bothell, WA, USA). The transducer positioned at the base of a water tank and focused at 45 mm. The water that filled the tank were distilled and degassed. The transmitted waveform was generated using a transducer power output unit (TPO-200, Sonic Concepts). The TPO unit combined an arbitrary waveform generator and a radiofrequency amplifier. A 30 s insonation treatment at a center frequency of 250 kHz was performed on each tube at PNP that ranged from 200 to 1350 kPa. To calibrate the transmitted pressure, measurements were conducted using a calibrated needle hydrophone (NH0500, Precision Acoustics, UK).

5.4. Sonoporation experiments

Fluorescent molecules with a size ranging from 1.2 kDa to 70 kDa were employed to assess the delivery to 4T1 breast cancer cells. 7-Aminoactinomycin D (7-AAD) (Thermo Fisher Scientific, A1310), a 1.2 kDa fluorescent dye that exhibits a spectral shift when it binds to DNA, Fluorescein isothiocyanate–dextran average molecular weights 4 kDa (FITC-Dextran 4) (46944, Sigma-Aldrich), FITC-Dextran 20 kDa (Sigma-Aldrich, FD20), and FITC-Dextran 70 kDa (Sigma-Aldrich, 46945) were the investigated fluorescent molecules for sonoporation (5 μg ml^{-1} 7-AAD or 1 mg ml^{-1} FITC-dextran). For the 7-AAD and FITC-Dextran 4 kDa experiments, the US

treatment was conducted immediately after the addition of the fluorescent material to the 0.5 ml Eppendorf tube, in order to avoid undesirable cellular uptake due to the molecules' small size. A mixture of 2.5×10^5 cells, sonoporated material and NBs, MBs or TMBs (at various tested concentrations, as described below) was transferred to 0.5 mL Eppendorf tubes. Subsequently, degassed PBS+/+ was added to achieve a final volume of 0.48 mL and a 250 kHz US treatment was then applied to the tubes, using the previously described low frequency US setup, with a pulse repetition frequency of 30 Hz and a 1.56 ms burst length. In the 7-AAD sonoporation experiments, after US insonation, Hoechst (33342, Abcam) was added to the tube to enable total cell counting of the sample (at a concentration of 10 μg ml^{-1}). Subsequently, the suspension was transferred to a 35 mm cell culture dish (430165, Corning) and examined under a fluorescence microscope (10× magnification). Imaging of the cells was performed using a bright field, a DAPI filter, and a mCherry filter. For analysis, a total of seven images were captured from different locations within the culture dish.

In the FITC-Dextran sonoporation experiments, the FITC molecules need to be present in the suspension during sonoporation, which induces the formation of pores in the cell membrane. Following US sonoporation, the cells were transferred to a pre-prepared 24-well plate (3526, Corning) filled with 300 μl of complete culture media (2.5% penicillin–streptomycin). The plate was subsequently placed in a humid 5% CO_2 incubator and incubated at 37 °C for a duration of 24 hours. Each well was then thoroughly rinsed three times with PBS+/+ to remove non-delivered FITC molecules, and then media were added. The cellular uptake and viability were visualized and quantified using the IncuCyte Live-Cell Analysis System (Essen Bioscience). Each group's experiments were performed in triplicate. For the NB optimizations experiments, a consistent treatment duration of 30 seconds was administered. This treatment duration was optimized in a previous study.[19] For NB concentration optimization, the concentrations tested were 1.29×10^7 NBs per μL (1×), 2.58×10^7 NBs per μL (2×), 5.16×10^7 NBs per μL (4×), 1.03×10^8 NBs per μL (8×), 1.55×10^8 NBs per μL (12×) and 2.06×10^8 NBs per μL (16×). The control groups were composed of a sham group, Free MB (mixed) + US at a concentration of 50 MB per cell, US treatment only and NB only (using the optimal NB concentration of 1.55×10^8 NBs per μL). In the free MB experiments, the MB suspension was mixed immediately before US application to increase the proximity between the MB and the cells. In the FITC 4 kDa, 20 kDa and 70 kDa sonoporation experiments, the TMBs were added to the cell mixtures at a concentration of 50 TMB/cell as described in.[32,33]

5.5. Data analysis

To analyze the 7-AAD sonoporation experiments, the following steps were performed using the ImageJ software: each microscope image was uploaded, the image type was converted to 16-bit, the threshold was adjusted to enhance the visibility of the stained cells and remove the background. Each experiment was performed in triplicate, with a total of 7 images captured in each repetition, resulting in 21 images analyzed for each group. The fraction of fluorescent cells was determined by calculating the percentage of 7-AAD-stained cells (red) divided by the total number of cells (Hoechst-blue-stained cells). The FITC sonoporation experiments were analyzed using the IncuCyte Live-Cell Analysis System (Essen Bioscience). For each well, sampling was carried out 25 times at a magnification of 20×. The calculation involved normalizing the green confluence (green cell area) by the phase confluence (total cell area). GraphPad Prism 9 software was utilized for statistical analysis. Significance was determined for P values <0.05, which were adjusted for multiple comparisons as specified in the figure captions. The results are presented as the mean ± SD.

Author contributions

Conceptualization, T.I.; methodology, T.I., M.E. and M.B.; validation, M.B. and M.E.; formal analysis, M.B.; investigation, M. B. and M.E.; resources, T.I.; writing – original draft preparation, M.B.; writing – review and editing, T.I.; visualization, M.B.; supervision, T.I.; project administration, T.I.; funding acquisition, T.I. All authors have read and agreed to the published version of the manuscript.

Conflicts of interest

There are no conflicts to declare.

Acknowledgements

This work was supported by the Israel Science Foundation (Grant Numbers 192/22 and 3450/20), the Israel Ministry of Science & Technology (Grant Number 101716), an ERC StG Grant No. 101041118 (NanoBubbleBrain), the Marian Gertner Institute and the Yoran Institute for Human Genome Research.

References

1 J. Foiret, H. Zhang, T. Ilovitsh, L. Mahakian, S. Tam and K. W. Ferrara, *Sci. Rep.*, 2017, **7**, 1–12.
2 B. Glickstein, H. Shinar and T. Ilovitsh, *Acoustic Technologies in Biology and Medicine*, 2023, 159–180.
3 T. Ilovitsh, Y. Feng, J. Foiret, A. Kheirolomoom, H. Zhang, E. S. Ingham, A. Ilovitsh, S. K. Tumbale, B. Z. Fite, B. Wu, M. N. Raie, N. Zhang, A. J. Kare, M. Chavez, L. S. Qi, G. Pelled, D. Gazit, O. Vermesh, I. Steinberg, S. S. Gambhir and K. W. Ferrara, *Proc. Natl. Acad. Sci. U. S. A.*, 2020, **117**, 12674–12685.
4 D. Sharma, K. X. Leong and G. J. Czarnota, *Int. J. Mol. Sci.*, 2022, **23**, 4393.

5 I. Lentacker, I. De Cock, R. Deckers, S. C. De Smedt and C. T. W. Moonen, *Adv. Drug Delivery Rev.*, 2014, **72**, 49–64.
6 Y. Yang, Q. Li, X. Guo, J. Tu and D. Zhang, *Ultrason. Sonochem.*, 2020, **67**, 105096.
7 Y. Z. Zhao, Y. K. Luo, C. T. Lu, J. F. Xu, J. Tang, M. Zhang, Y. Zhang and H. D. Liang, *J. Drug Targeting*, 2008, **16**, 18–25.
8 J. Tu and A. C. H. Yu, *BME Front.*, 2022, DOI: **10.34133/2022/9807347**.
9 Y. Negishi, Y. Endo-Takahashi and K. Maruyama, *Drug Discoveries Ther.*, 2016, **10**, 248–255.
10 A. Delalande, C. Bastié, L. Pigeon, S. Manta, M. Lebertre, N. Mignet, P. Midoux and C. Pichon, *Biosci. Rep.*, 2017, **37**, DOI: **10.1042/BSR20160619**.
11 S. Kotopoulis, G. Dimcevski and O. H. Gilja, *Textb. Pancreat. Cancer Princ. Pract. Surg. Oncol*, 2021, pp. 1281–1292.
12 K. A. Stewart, S. M. Navarro, S. Kambala, G. Tan, R. Poondla, S. Lederman, K. Barbour and C. Lavy, *Int. J. Matern. Child Health AIDS*, 2020, **9**, 103.
13 T. Di Ianni, R. J. C. Bose, U. K. Sukumar, S. Bachawal, H. Wang, A. Telichko, C. Herickhoff, E. Robinson, S. Baker and J. G. Vilches-Moure, *J. Controlled Release*, 2019, **309**, 1–10.
14 Z. Xu, T. L. Hall, E. Vlaisavljevich and F. T. Lee Jr., *Int. J. Hyperthermia*, 2021, **38**, 561–575.
15 A. J. Dixon, J. P. Kilroy, A. H. Dhanaliwala, J. L. Chen, L. C. Phillips, M. Ragosta, A. L. Klibanov, B. R. Wamhoff and J. A. Hossack, *IEEE Trans. Ultrason. Ferroelectr. Freq. Control*, 2015, **62**, 1674–1685.
16 A. L. Klibanov, *Invest. Radiol.*, 2021, **56**, 50–61.
17 C. Pellow, D. E. Goertz and G. Zheng, *Wiley Interdiscip. Rev.: Nanomed. Nanobiotechnol.*, 2018, **10**, DOI: **10.1002/wnan.1502**.
18 R. Cavalli, M. Soster and M. Argenziano, *Ther. Delivery*, 2016, **7**, 117–138.
19 M. Bismuth, S. Katz, T. Mano, R. Aronovich, D. Hershkovitz, A. A. Exner and T. Ilovitsh, *Nanoscale*, 2022, **14**, 13614–13627.
20 Y. Wang, X. Li, Y. Zhou, P. Huang and Y. Xu, *Int. J. Pharm.*, 2010, **384**, 148–153.
21 Y. Endo-Takahashi and Y. Negishi, *Pharmaceutics*, 2020, **12**, 964.
22 A. Delalande, S. Kotopoulis, M. Postema, P. Midoux and C. Pichon, *Gene*, 2013, **525**, 191–199.
23 H. Kida, K. Nishimura, K. Ogawa, A. Watanabe, L. B. Feril, Y. Irie, H. Endo, S. Kawakami and K. Tachibana, *Front. Pharmacol.*, 2020, **11**, 363.
24 D. V. B. Batchelor, F. J. Armistead, N. Ingram, S. A. Peyman, J. R. McLaughlan, P. L. Coletta and S. D. Evans, *Langmuir*, 2022, **38**, 13943–13954.
25 P. A. Payne, *J. Phys. E: Sci. Instrum.*, 1985, **18**, 465.
26 B. Helfield, Y. Zou and N. Matsuura, *Front. Phys.*, 2021, **9**, 654374.
27 S. Qin and K. W. Ferrara, *Ultrasound Med. Biol.*, 2007, **33**, 1140–1148.
28 A. Harkin, A. Nadim and T. J. Kaper, *Phys. Fluids*, 1999, **11**, 274–287.
29 F. G. Blake, *The onset of cavitation in liquids: I*, Harvard University, Tech. Memo, 1949.
30 W. Lauterborn, *J. Acoust. Soc. Am.*, 1976, **59**, 283–293.
31 T. Ilovitsh, A. Ilovitsh, J. Foiret, C. F. Caskey, J. Kusunose, B. Z. Fite, H. Zhang, L. M. Mahakian, S. Tam, K. Butts-Pauly, S. Qin and K. W. Ferrara, *Sci. Rep.*, 2018, **8**, 1–15.
32 M. Bismuth, S. Katz, H. Rosenblatt, M. Twito, R. Aronovich and T. Ilovitsh, *Bioconjugate Chem.*, 2021, 1069–1079.
33 M. Eck, R. Aronovich and T. Ilovitsh, *Int. J. Pharm.: X*, 2022, **4**, 100132.
34 R. Haugse, A. Langer, E. T. Murvold, D. E. Costea, B. T. Gjertsen, O. H. Gilja, S. Kotopoulis, G. Ruiz de Garibay and E. McCormack, *Pharmaceutics*, 2020, **12**, 1058.
35 H. Tsai, L. Liu, G. J. Dusting, W. Weng, S. Chen, M. Kung, R. Tee, G. Liu and M. Tai, *J. Gene Med.*, 2012, **14**, 44–53.
36 A. C. Huang, M. A. Postow, R. J. Orlowski, R. Mick, B. Bengsch, S. Manne, W. Xu, S. Harmon, J. R. Giles and B. Wenz, *Nature*, 2017, **545**, 60–65.
37 J. Gerritsen, L. Arends, M. Klimek, C. Dirven and A. Vincent, *Acta Neurochir.*, 2019, **161**, 99–107.
38 P. Wawryka, A. Kiełbik and G. Iwanek, *Med. Res. J.*, 2019, **4**, 178–183.
39 D. L. Miller, S. Bao and J. E. Morris, *Ultrasound Med. Biol.*, 1999, **25**, 143–149.
40 R. Karshafian, S. Samac, P. D. Bevan and P. N. Burns, *Ultrasonics*, 2010, **50**, 691–697.
41 R. Karshafian, P. D. Bevan, R. Williams, S. Samac and P. N. Burns, *Ultrasound Med. Biol.*, 2009, **35**, 847–860.
42 B. D. M. Meijering, L. J. M. Juffermans, A. van Wamel, R. H. Henning, I. S. Zuhorn, M. Emmer, A. M. G. Versteilen, W. J. Paulus, W. H. van Gilst and K. Kooiman, *Circ. Res.*, 2009, **104**, 679–687.
43 J. Rich, Z. Tian and T. J. Huang, *Adv. Mater. Technol.*, 2022, **7**, 2100885.
44 S. Kotopoulis, A. Delalande, M. Popa, V. Mamaeva, G. Dimcevski, O. H. Gilja, M. Postema, B. T. Gjertsen and E. McCormack, *Mol. Imaging Biol.*, 2014, **16**, 53–62.
45 J. N. Belling, L. K. Heidenreich, Z. Tian, A. M. Mendoza, T.-T. Chiou, Y. Gong, N. Y. Chen, T. D. Young, N. Wattanatorn and J. H. Park, *Proc. Natl. Acad. Sci. U. S. A.*, 2020, **117**, 10976–10982.
46 G. Shapiro, A. W. Wong, M. Bez, F. Yang, S. Tam, L. Even, D. Sheyn, S. Ben-David, W. Tawackoli and G. Pelled, *J. Controlled Release*, 2016, **223**, 157–164.
47 R. Karshafian, *On the permeabilisation and disruption of cell membranes by ultrasound and microbubbles*, University of Toronto, 2010.
48 Y. S. Li, E. Davidson, C. N. Reid and A. P. McHale, *Cancer Lett.*, 2009, **273**, 62–69.
49 A. V. Telichko, H. Wang, S. Bachawal, S. U. Kumar, J. C. Bose, R. Paulmurugan and J. J. Dahl, *Ultrasound Med. Biol.*, 2021, **47**, 309–322.
50 K. Hynynen and F. A. Jolesz, *Ultrasound Med. Biol.*, 1998, **24**, 275–283.

51 A. Carovac, F. Smajlovic and D. Junuzovic, *Acta Inform. Med.*, 2011, **19**, 168.
52 X. Yin and K. Hynynen, *Phys. Med. Biol.*, 2005, **50**, 1821.
53 S. Schoen Jr., M. S. Kilinc, H. Lee, Y. Guo, F. L. Degertekin, G. F. Woodworth and C. Arvanitis, *Adv. Drug Delivery Rev.*, 2022, **180**, 114043.
54 A. N. Pouliopoulos, S.-Y. Wu, M. T. Burgess, M. E. Karakatsani, H. A. S. Kamimura and E. E. Konofagou, *Ultrasound Med. Biol.*, 2020, **46**, 73–89.
55 C. Gasca-Salas, B. Fernández-Rodríguez, J. A. Pineda-Pardo, R. Rodríguez-Rojas, I. Obeso, F. Hernández-Fernández, M. Del Álamo, D. Mata, P. Guida and C. Ordás-Bandera, *Nat. Commun.*, 2021, **12**, 779.
56 B. Z. Fite, J. Wang, A. J. Kare, A. Ilovitsh, M. Chavez, T. Ilovitsh, N. Zhang, W. Chen, E. Robinson, H. Zhang, A. Kheirolomoom, M. T. Silvestrini, E. S. Ingham, L. M. Mahakian, S. M. Tam, R. R. Davis, C. G. Tepper, A. D. Borowsky and K. W. Ferrara, *Sci. Rep.*, 2021, **11**, 1–15.
57 M. Maciulevičius, M. Tamošiūnas, D. Navickaitė, S. Šatkauskas and M. S. Venslauskas, *J. Drug Delivery Sci. Technol.*, 2022, **72**, 103386.
58 X. Liu, F. Wu, Y. Ji and L. Yin, *Bioconjugate Chem.*, 2018, **30**, 305–324.
59 M. R. Dreher, W. Liu, C. R. Michelich, M. W. Dewhirst, F. Yuan and A. Chilkoti, *J. Natl. Cancer Inst.*, 2006, **98**, 335–344.
60 W. Matsunaga, M. Ichikawa, A. Nakamura, T. Ishikawa and A. Gotoh, *Anticancer Res.*, 2018, **38**, 2015–2020.
61 Y. Tian, Z. Liu, H. Tan, J. Hou, X. Wen, F. Yang and W. Cheng, *Int. J. Nanomed.*, 2020, 401–418.
62 Y. U. Wang, Y. Chen, W. Zhang, Y. U. Yang, W. Bai, E. Shen and B. Hu, *Oncol. Lett.*, 2016, **11**, 699–704.
63 Z. Fan, R. E. Kumon and C. X. Deng, *Ther. Delivery*, 2014, **5**, 467–486.
64 J. N. Meegoda, S. Aluthgun Hewage and J. H. Batagoda, *Environ. Eng. Sci.*, 2018, **35**, 1216–1227.
65 J. Park, Z. Fan and C. X. Deng, *J. Biomech.*, 2011, **44**, 164–169.
66 R. Perera, C. Hernandez, M. Cooley, O. Jung, S. Jeganathan, E. Abenojar, G. Fishbein, A. J. Sojahrood, C. C. Emerson and P. L. Stewart, *Nanoscale*, 2019, **11**, 15647–15658.